Discrete Lyapunov Controllers for an Actuator in Camless Engines

Paolo Mercorelli and Nils Werner

***Abstract*—This paper deals with a hybrid actuator composed by a piezo and a hydraulic part controlled using two cascade Lyapunov controllers for camless engine motor applications. The idea is to use the advantages of both, the high precision of the piezo and the force of the hydraulic part. In fact, piezoelectric actuators (PEAs) are commonly used for precision positionings, despite PEAs present nonlinearities, such as hysteresis, saturations, and creep. In the control problem such nonlinearities must be taken into account. In this paper the Preisach dynamic model with the above mentioned nonlinearities is considered together with cascade controllers which are Lyapunov based. The sampled control laws are derived using the well known Backward Euler method. An analysis of the Backward and Forward Euler method is also presented. In particular, the hysteresis effect is considered and a model with a switching function is used also for the controller design. Simulations with real data are shown.**

***Index Terms*—Lyapunov approach, hybrid actuators.**

I. Introduction

Recently, variable engine valve control has attracted a lot of attention because of its ability to improve fuel economy, reduce NOx emissions and to increase torque performance over a wider range than a conventional spark-ignition engine. In combination with microprocessor control, key functions of the motor management can be efficiently controlled by such mechatronic actuators. For moving distances between 5 and 8 mm, however, there are many actuator types with different advantages and drawbacks. We presented an adaptive PID controller design for a valve actuator control. In [1] a U-magnet structure is considered in which the Maxwell attracting force is quadratic to the current and inversely quadratic to the distance between the valve armature and the electromagnets. Using the topology presented in [1], it is possible to have the availability of a very big force with a small current. Nevertheless, difficulties connected with the control structure and in particular with the control for high cycles of the motor encouraged us to test other topologies. The main idea of this paper is using a hybrid actuator consisting of a piezo and a hydraulic part in order to take advantages of both of them: the high precision and velocity of the piezo and the force of the hydraulic part. Hydraulic actuators have been an attractive field since many years. Recently in [2] a nonlinear model of a hydraulic actuator considering amplitude and rate saturations, identified by an innovative method is proposed. An actuator model is taken into account with a first-order transfer function and nonlinear functions of saturation with unknown parameters. Piezo actuators demonstrate generally less difficulties of electromagnetic compatibility due to the quasi-absence of the inductance effects. The objective of this paper is to show a model of a hybrid actuator and a Lyapunov cascade regulator using, in one case, the Forward Euler discrete approximation, and finally, the case of Backward Euler approximation. The paper is organized with the following sections. Section II is devoted to the model description. After that, in Section III and IV, the control laws are derived. The paper ends with Section V in which simulation results of the proposed valve using real data are presented. After that, the conclusions follow.

Paolo Mercorelli is with the Institute of Product and Process Innovation, Leuphana University of Lueneburg, Volgershall 1, D-21339 Lueneburg, Germany. Phone: +49-(0)4131-677-5571, Fax: +49-(0)4131-677-5300. mercorelli@uni.leuphana.de. Nils Werner is with the Faculty of Automotive Engineering, Ostfalia University of Applied Sciences, Kleiststr. 14-16, D-38440 Wolfsburg, Germany. Phone: +49-(0)5361-831615 Fax. +49-(0)5361-831602. n.werner@ostfalia.de

The main nomenclature

$V_{in}(t)$: input voltage
$V_z(t)$: internal piezo voltage
$i(t)$: piezo input current
R_0: input resistance in the piezo model
R_a: parasite resistance in the piezo model
C_a: parasite capacitance in the piezo model
C_z: internal capacitance in the piezo model
$x_p(t)$: internal position of the piezo part
$x(t) = x_1(t)$: position of the piezo mass
$\dot{x}(t) = x_2(t)$: velocity of the piezo mass
$H(x_p(t), V_{in}(t))$: hysteresis characteristic of the piezo
$M_p/3$: moving piezo mass
K_x: internal spring constant of the piezo
K: spring constant acting on the piezo
D: damping constant acting on the piezo
D_{oil}: damping constant of the oil chamber acting on the piezo
$x_{SK}(t)$: position of the servo piston
$M_{SK}(t)$: mass of the servo piston
$K_{SK}(t)$: spring constant acting on the servo piston
$D_{SK}(t)$: damping constant acting on the servo piston
W: piezo$\rightarrow$ servopiston ratio
Q_{th}: mass flux of the hydraulic part
T_H: time constant of the linear model of the hydraulic part
T_M: time constant of the linear model of the mechanical part
V_H: steady-state factor of the linear model of the hydraulic part
V_M: steady-state factor constant of the linear model of the mechanical part
$K2Lidx$: characteristic value of the velocity-dependent internal leakage
T_s: sampling time

II. Modeling of the piezo hydraulic actuator

In the diagram of Fig. 1 the T-A connection links the couple of valves with the tank and the P-B connection links the couple of valves with the pump. In the position of Fig. 1 connections T-A and P-B are maximally open and the couple of valves are closed because point B is under pressure. When the piezo acts its force, the mechanical servo valve moves and begins to close these connections. When the mechanical servo valve is in the middle position, both connections (T-A and P-B) are closed and connections A-P and B-T begin to open. At this position also both motor valves begin to open because point A is under pressure. Figure 1 shows in detail a part of the hybrid structure

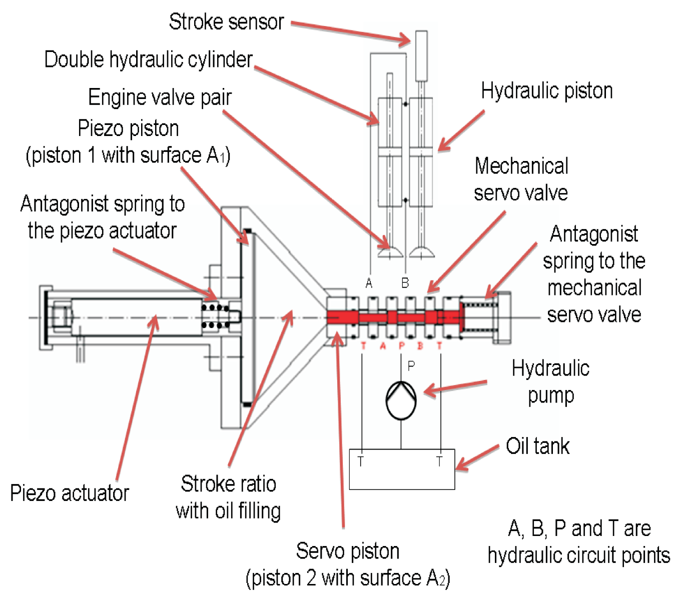

Fig. 1. Scheme of the whole Hybrid Piezo Hydraulic structure

which consists of a piezo actuator combined with a mechanical part. These two parts are connected by a stroke ratio to adapt the stroke length. The proposed nonlinearity model for PEA is quite similar to these presented in [3] and in [4] which show a sandwich model for a PEA. According to this proposed sandwich model, a PEA is constituted like a three layer sandwich. The middle layer is the effective piezo layer (P-layer), and the two outside layers connected to the electrodes are known in the literature as interfacing layers (I-layers). The P-layer is the layer that has the ordinary characteristics of piezo effects but without the nonlinearities of hysteresis and creep so that its behavior can be modeled by an equivalent linear circuitry. In contrast, the I-layers do not contribute any piezo effect; they are just parts of the circuit connecting P-layer to the electrodes in series. In [4] it is hypothesized that each of the I-layers can be equivalently represented by a capacitor and a resistor connected together in parallel. Together with the equivalent circuitry for P-layer, Fig. 2 shows the equivalent circuitry for a PEA with the I-layer nonlinearities of hysteresis and creep, in which two I-layers are combined together as C_a and R_a. The I-layer capacitor, C_a, is an ordinary one, which might be varied slightly with some factors, but here it would be assumed constant first for simplicity. The I-

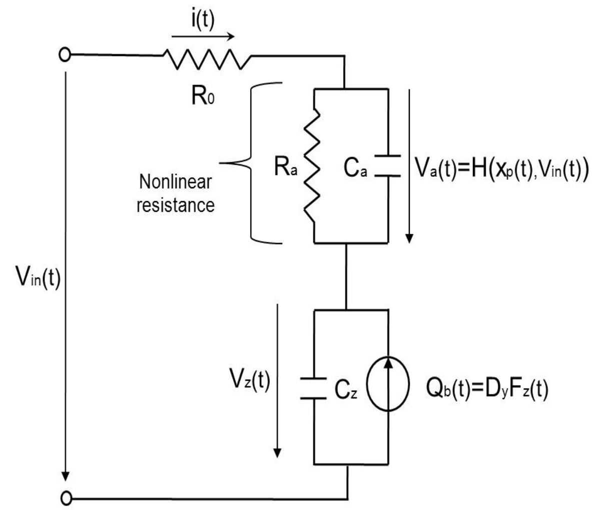

Fig. 2. Electrical part of the model

layer resistor, R_a , however, is really an extraordinary one with a significant nonlinearity. The resistance is either fairly large, say $R_a > 10^6\ \Omega$, when the voltage $\|V_a\| < V_h$, or is fairly small, say $R_a < 1000$, when $\|V_a\| > V_h$. In [4], the threshold voltage, V_h, is defined as the hysteresis voltage of a PEA. The authors in [4] gave this definition due to the observation that there is a significant difference and an abrupt change in resistance across this threshold voltage and it is this resistance difference and change across V_h that introduces the nonlinearities of hysteresis and creep in a PEA. The hysteresis effect could be seen as a function of input $V_{in}(t)$ and output $y(t)$ as follows: $H(y(t), V_{in}(t))$, see Fig. 3. According to this model, if $V_h = 0$, then the hysteresis will disappear, and if $R_a = \infty$ when $\|V_a\| < V_h$, then the creep will also disappear. Based on this proposed sandwich model and the equivalent circuitry as shown in Fig. 2, we can further derive the state model as follows:

$$\dot{V}_a(t) = -\Big(\frac{1}{R_a} + \frac{1}{R_o}\Big)\frac{V_a(t)}{C_a} - \frac{V_z(t)}{C_a R_o} + \frac{V_{in}(t)}{C_a R_o} \quad (1)$$

$$\dot{V}_z(t) = \frac{\dot{Q}_b}{C_z} + \frac{1}{C_z}\Big(-\frac{V_a(t)}{R_o} - \frac{V_z(t)}{R_o} + \frac{V_{in}(t)}{R_o}\Big), \quad (2)$$

where $Q_b = D_y F_z(t)$ is the "back electric charge force" (back-ecf) in a PEA, see [4]. According to [4] and the notation of Fig. 4, it is possible to write:

$$F_z(t) = M_p/3\ddot{x}(t) + D\dot{x}(t) + Kx(t) + K_x x(t). \quad (3)$$

K and D are the elasticity and the friction constant of the spring which is antagonist to the piezo effect and is incorporated in the PEA. C_z is the total capacitance of the PEA and R_o is the contact resistance. For further details on this model see [4]. Considering the whole system described in Fig. 4 with the assumptions of incompressibility of the oil, the whole mechanical system can be represented by a spring mass structure as shown in the conceptual scheme of Fig. 4. In this system the following notation is adopted: K_x

ISBN: 978-1-61804-216-3

is the elasticity constant factor of the PEA. In the technical literature, factor $D_x K_x = T_{em}$ is known with the name "transformer ratio" and states the most important characteristic of the electromechanical transducer. $M_p/3$ is, in our case, the moving mass of the piezo structure which is a fraction of whole piezo mass, M_{SK} is the sum of the mass of the piston with the oil and the moving actuator and M_v is the mass of the valve. It is possible to notice that the moving mass of the piezo structure is just a fraction of the whole piezo mass. The value of this fraction is given by the constructer of the piezo device and it is determined by experimental measurements. K_{SK} and D_{SK} are the characteristics of the antagonist spring to the mechanical servo valve, see Fig. 4. D_{oil} is the friction constant of the oil. Moreover, according to [4], motion $x_p(t)$ of diagram in Fig. 3 is:

$$x_p(t) = D_x V_z(t). \quad (4)$$

According to diagram of Fig. 2, it is possible to write as follows:

$$V_z = V_{in}(t) - R_0 i(t) - H(x_p(t), V_{in}(t)), \quad (5)$$

where R_0 is the connection resistance and $i(t)$ is the input current as shown in Fig. 2. $H(x_p(t), V_{in}(t))$ is the function which describes the hysteresis effect mentioned above and shown in the simulation of Fig. 3. Considering the whole system described in Fig. 4, the electrical and mechanical systems described in Figs. 2, 3 and 4 can be represented by the following mathematical expressions:

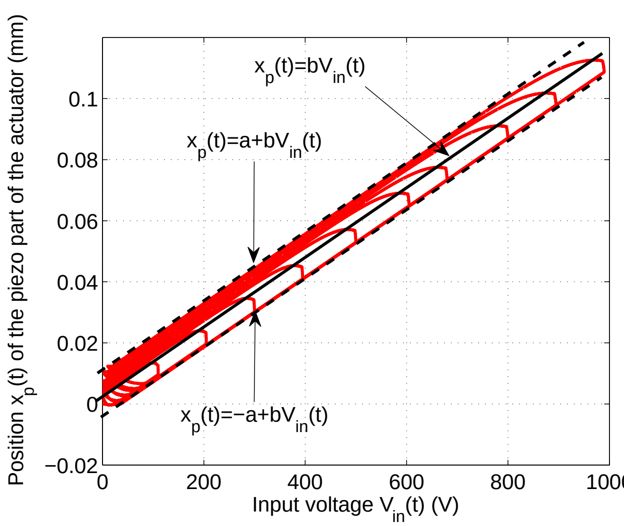

Fig. 3. Simulated Hysteresis curve of the piezo part of the actuator: $H(x_p(t), V_{in}(t))$

$$\frac{M_p}{3}\ddot{x}(t) + M_{SK}\ddot{x}_{SK}(t) + Kx(t) + D\dot{x}(t) + K_{SK}x_{SK}(t) + D_{SK}\dot{x}_{SK}(t) + D_{oil}\dot{x}_{SK}(t) + K_x\Big(x(t) - \Delta x_p(V_{in}(t))\Big) = 0, \quad (6)$$

where $\Delta x_p(t)$ represents the interval function of $x_p(t)$ as shown in Fig. 3 which, according to equation (4), can be expressed as:

$$\Delta x_p(t) = D_x \Delta V_z(t). \quad (7)$$

Finally, using equations (5) and (7),

$$K_x \Delta x_p(t) = K_x D_x\big(V_{in}(t) - R_0 i(t) - H(\Delta x_p(t), V_{in}(t))\big), \quad (8)$$

which represents the interval force generated by the piezo device. Equation (6) can be expressed in the following way:

$$\frac{M_p}{3}\ddot{x}(t) + M_{SK}\ddot{x}_{SK}(t) + Kx(t) + D\dot{x}(t) + K_{SK}x_{SK}(t) + D_{SK}\dot{x}_{SK}(t) + D_{oil}\dot{x}_{SK}(t) + K_x x(t) = K_x\Delta x_p(V_{in}(t)). \quad (9)$$

It is to be noticed that under quasi-static conditions (low velocity ranges) the following relation holds:

$$x_{SK}(t) \approx W x(t), \quad (10)$$

where W is the position ratio above defined and it states the incompressibility of the oil in the conic chamber. $F_d(t)$ is the combustion back pressure in terms of force. According to Fig. 3 in which an upper bound and a lower bound of the hysteresis curve are indicated, it is possible to write that:

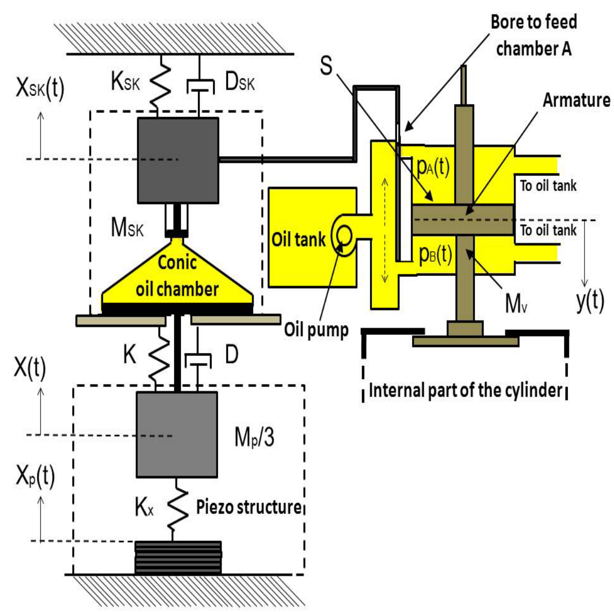

Fig. 4. Mass spring model of the whole actuator

$$\Delta x_p(V_{in}(t)) = [-a \quad a] + bV_{in}(t), \quad (11)$$

with $a \in \mathbb{R}$ and $b \in \mathbb{R}$ two positive constants are indicated. In particular,

$$\underline{\Delta} x_p(V_{in}(t)) = -a + bV_{in}(t), \quad (12)$$

and

$$\overline{\Delta} x_p(V_{in}(t)) = a + bV_{in}(t). \quad (13)$$

Considering this notation, the system represented in (6) can be split into the following two models:

$$\frac{M_p}{3}\ddot{x}(t) + M_{SK}\ddot{x}_{SK}(t) + Kx(t) + D\dot{x}(t) + K_{SK}x_{SK}(t) + D_{SK}\dot{x}_{SK}(t) + D_{oil}\dot{x}_{SK}(t) + K_x x(t) = \underline{\Delta} x_p(V_{in}(t)), \quad (14)$$

ISBN: 978-1-61804-216-3

and

$$\frac{M_p}{3}\ddot{x}(t)+M_{SK}\ddot{x}_{SK}(t)+Kx(t)+D\dot{x}(t)+K_{SK}x_{SK}(t)+ D_{SK}\dot{x}_{SK}(t)+D_{oil}\dot{x}_{SK}(t)+K_x x(t)=\overline{\Delta}x_p(V_{in}(t)), \quad (15)$$

III. CONTROL OF THE PIEZO MECHANICAL PART OF THE ACTUATOR

If $x(t)=x_1(t)$, then:

$$\begin{aligned}\dot{x}_1(t) &= x_2(t) &(16)\\ \dot{x}_2(t) &= \frac{-Dx_2(t)-W(D_{SK}+D_{oil})x_2(t)}{\frac{M_p}{3}+M_{SK}W}+ \\ &\frac{-(K+K_x+K_{SK}W)x_1(t)}{\frac{M_p}{3}+M_{SK}W}+ \\ &\frac{3K_x bV_{in}(t)+(-1)^q a}{\frac{M_p}{3}+M_{SK}W}, &(17)\end{aligned}$$

where $q=1,2$. If it is assumed that $V_{in}(t)=V_z(t)$, then

$$\begin{bmatrix}\dot{x}_{1_{SK}}(t)\\ \dot{x}_{2_{SK}}(t)\end{bmatrix}=\begin{bmatrix}0 & 1\\ -\frac{c_n}{a_n} & -\frac{b_n}{a_n}\end{bmatrix}\cdot\begin{bmatrix}x_1(t)\\ x_2(t)\end{bmatrix}+ \begin{bmatrix}0\\ \frac{3K_x b}{a_n}\end{bmatrix}\cdot\left[V_z(t)+\frac{a(-1)^q}{3K_x b}\right], \quad (18)$$

where

$$a_n=\frac{M_P}{3}+M_{SK}\cdot W \quad (19)$$

$$b_n=D+D_{SK}\cdot W \quad (20)$$

$$c_n=K_x+K+K_{SK}\cdot W. \quad (21)$$

To sum up, it is possible to write the following general expression for the dynamics of the piezo part of the actuator:

$$\dot{\mathbf{x}}(t)=\mathbf{A}_n\cdot\mathbf{x}(t)+\mathbf{B}_n\cdot\left[V_z(t)+\frac{a(-1)^q}{3K_x b}\right]. \quad (22)$$

To obtain the servo piston position it is enough to remember that in quasi-static conditions the following expressions hold: $x_{SK}(t)\approx Wx_1(t)$ and $\dot{x}_{SK}(t)\approx Wx_2(t)$.

A. A Lyapunov based controller for the piezo mechanic actuator

For designing a controller for the piezo mechanical part of the actuator, it is to consider that, according to the real data which we have, the piezo part of the model results to be more than 10 times faster than the mechanical part. This allows us to consider just the mechanical model in order to conceive a possible control law. Considering $\mathbf{K}_i(t)=\mathbf{e}(t)=\mathbf{x}_d(t)-\mathbf{x}(t)$, in which $\mathbf{x}_d(t)$ represents the desired state vector (position and velocity) of the servo mechanical piston. Defining

$$\mathbf{V}(\mathbf{K}_i)=\frac{\mathbf{K}_i^2(t)}{2}, \text{then it follows that:} \quad (23)$$

$$\dot{\mathbf{V}}(\mathbf{K}_i)=\mathbf{K}_i(t)\dot{\mathbf{K}}_i(t). \quad (24)$$

In order to find a stabile solution, it is possible to choose the following function:

$$\dot{\mathbf{V}}(\mathbf{K}_i)=-\eta(t){\mathbf{K}_i}^2(t), \quad (25)$$

with η a positive definite diagonal matrix is indicated. Comparing (24) with (25), the following relationship is obtained:

$$\mathbf{K}_i(t)\dot{\mathbf{K}}_i(t)=-\eta\mathbf{K}_i^2(t), \quad (26)$$

and finally

$$\mathbf{K}_i(t)\big(\dot{\mathbf{K}}_i(t)+\eta\mathbf{K}_i(t)\big)=0. \quad (27)$$

The no trivial solution follows from the condition

$$\dot{\mathbf{K}}_i(t)+\eta\mathbf{K}_i(t)=0, \quad (28)$$

which can be rewritten as:

$$\dot{\mathbf{x}}_d(t)-\dot{\mathbf{x}}(t)+\eta\big(\mathbf{x}_d(t)-\mathbf{x}(t)\big)=0. \quad (29)$$

Considering Eq. (22) the following expression is obtained:

$$\dot{\mathbf{x}}_d(t)-\mathbf{A}_n\cdot\mathbf{x}(t)+\mathbf{B}_n\cdot\left[V_z(t)+\frac{a(-1)^q}{3K_x b}\right]+ \eta\big(\mathbf{x}_d(t)-\mathbf{x}(t)\big)=0, \quad (30)$$

it follows that:

$$V_z(t)=pinv(\mathbf{B}_n)\cdot \Big(\mathbf{A}_n\cdot\mathbf{x}(t)-\dot{\mathbf{x}}_d(t)-\eta\big(\mathbf{x}_d(t)+\mathbf{x}(t)\big)\Big)-\frac{a(-1)^q}{3K_x b}, \quad (31)$$

where Moore-Penrose Pseudoinverse of matrix $\mathbf{B}_n$ is used. Considering that the model of Eq. (22) is a minimum phase model, then signal $V_z(t)$ is a limited one. Using the control of Eq. (31), the following error dynamics is obtained:

$$\dot{\mathbf{e}}(t)+\eta\mathbf{e}(t)=0. \quad (32)$$

If a non exact cancellation is considered, then:

$$\dot{\mathbf{e}}(t)+\eta\mathbf{e}(t)=\mathbf{\Delta}(\mathbf{x}_d(t),\mathbf{x}(t)), \quad (33)$$

where $\mathbf{\Delta}(\mathbf{x}_d(t),\mathbf{x}(t))$ represents the cancellation error which can be assumed to be limited because of model of Eq. (22) being a minimum phase one. Considering the Forward Euler sampling approximation, Eq. (33) becomes:

$$\mathbf{e}(k)-\mathbf{e}(k-1)+T_s\eta\mathbf{e}(k-1)=T_s\mathbf{\Delta}(\mathbf{x}_d(k-1),\mathbf{x}(k-1)), \quad (34)$$

where T_s equals the sampling time. It is well known that in order to obtain the asymptotic stability it must be $\eta < diag(2/T_s)$, but in this case parameter η does not influence the reduction of the error. In fact, we can write the following relation:

$$\mathbf{e}(k)=(\mathbf{I}-T_s\eta)\mathbf{e}(k-1)+T_s\mathbf{\Delta}(\mathbf{x}_d(k-1),\mathbf{x}(k-1)). \quad (35)$$

If Backward Euler sampling approximation is considered, then Eq. (33) becomes:

$$\mathbf{e}(k)-\mathbf{e}(k-1)+T_s\eta\mathbf{e}(k)=T_s\mathbf{\Delta}(\mathbf{x}_d(k),\mathbf{x}(k)), \quad (36)$$

and in case of no exact cancellation through parameter η it is possible to control the error: the bigger parameter η is, the smaller the error becomes. In fact, we can write the following relation:

$$\mathbf{e}(k)=(\mathbf{I}+T_s\eta)^{-1}\mathbf{e}(k-1)+ (\mathbf{I}+T_s\eta)^{-1}T_s\mathbf{\Delta}(\mathbf{x}_d(k-1),\mathbf{x}(k-1)). \quad (37)$$

If the Backward Euler sampling method is considered for the control law of Eq. (31), then:

$$V_z(k) = pinv(\mathbf{B}_n)\cdot\Big(\mathbf{A}_n\cdot\mathbf{x}(k) - \frac{\mathbf{x}_d(k)-\mathbf{x}_d(k-1)}{T_s} - \eta\big(\mathbf{x}_d(k)+\mathbf{x}(k)\big)\Big) - \frac{a(-1)^q}{3K_x b}, \quad (38)$$

where Moore-Penrose Pseudoinverse of $\mathbf{B}_n$ is used.

IV. Modelling and control of the hydraulic part of the actuator

In Fig. 5 a possible linear model often utilised in practical applications is presented. The model was presented in [5] and it is a possible linear approximation utilized in many industrial applications, see the industrial cases presented in [5]. In Fig. 5 this model in which, the following parameters are visible, is represented: T_H which represents the time constant of the hydraulic part, T_M which represents the time constant of the mechanic part. V_H and V_M represent the steady state factors of the hydraulic and mechanical transfer function respectively. The other parameter which characterises the hydraulic-mechanical model is $K2Lidx$. In fact, parameter $K2Lidx$ is a characteristic value of the velocity-dependent internal leakage. This parameter multiplied by the velocity of the valve states a loosing force as represented in the block diagram of Fig. 5. Parameter A_{AK} is the surface of the moving part (servo piston). Observing Fig. 5 and considering that

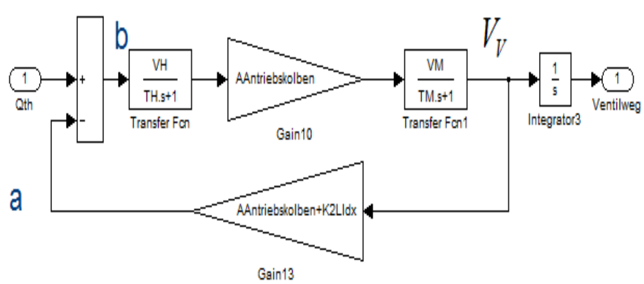

Fig. 5. Hydraulic model structure

variable Q_{th} is the mass flux involved in the hydraulic actuator, the following calculations are derived:

$$b_m = Q_{th}(s) - a_m \quad (39)$$

$$V_V(s) = b_m\cdot\frac{V_H\cdot V_M\cdot A_{AK}}{(T_H\cdot s+1)\cdot(T_M\cdot s+1)} \quad (40)$$

$$V_V(s) = b_m\cdot\frac{V_H\cdot V_M\cdot A_{AK}}{T_H\cdot T_M\cdot s^2+(T_H+T_M)\cdot s+1} \quad (41)$$

$$a_m = V_V(s)\cdot(A_{AK}+K2Lidx), \quad (42)$$

$$b_m = Q_{th}(s) - V_V(s)\cdot(A_{AK}+K2Lidx), \quad (43)$$

$$V_V(s) = (Q_{th}(s) - V_V(s)\cdot(A_{AK}+K2Lidx))\cdot\frac{V_H\cdot V_M\cdot A_{AK}}{T_H\cdot T_M\cdot s^2+(T_H+T_M)\cdot s+1} \quad (44)$$

Considering the transfer function, then:

$$\frac{V_V(s)}{Q_{th}(s)} = \frac{d_m}{a_m\cdot s^2+b_m\cdot s+c_m}, \quad (45)$$

where:

$$a_m = T_H\cdot T_M, \quad (46)$$

$$b_m = (T_H+T_M), \quad (47)$$

$$c_m = 1+V_H\cdot V_M\cdot A_{AK}\cdot(A_{AK}+K2Lidx), \quad (48)$$

$$d_m = V_H\cdot V_M\cdot A_{AK}, \quad (49)$$

$$a_m\cdot s^2\cdot V_V(s)+b\cdot s\cdot V_V(s)+c\cdot V_V(s)-d_m\cdot Q_{th}(s)=0. \quad (50)$$

Considering the back Laplace transform, then:

$$a_m\cdot\ddot{V}_V(t)+b\cdot\dot{V}_V(t)+c\cdot V_V(t)-d_m\cdot Q_{th}(t)=0. \quad (51)$$

If the following positions are considered:

$$x_1(t) = V_V(t) \quad (52)$$

$$x_2(t) = \dot{x}_1(t) \quad (53)$$

then:

$$\dot{x}_1(t) = x_2(t) \quad (54)$$

$$\dot{x}_2(t) = \frac{1}{a_m}\cdot(d_m\cdot Q_{th}(t) - b_m\cdot x_2(t) - c_m\cdot x_1(t)) \quad (55)$$

and

$$\begin{bmatrix}\dot{x}_1(t)\\ \dot{x}_2(t)\end{bmatrix} = \begin{bmatrix}0 & 1\\ -\frac{c_m}{a_m} & -\frac{b_m}{a_m}\end{bmatrix}\cdot\begin{bmatrix}x_1(t)\\ x_2(t)\end{bmatrix} + \begin{bmatrix}0\\ \frac{d_m}{a_m}\end{bmatrix}\cdot Q_{th}(t). \quad (56)$$

It is possible to write the following general equation:

$$\dot{\mathbf{x}}(t) = \mathbf{A}_m\cdot\mathbf{x}(t)+\mathbf{B}_m\cdot Q_{th}(t). \quad (57)$$

Concerning the control aspects, similar considerations as for the piezo mechanical part of the actuator can be done and the following sampled control law can be derived using Backward Euler sampling method, the following final inverse equation is obtained:

$$Q_{th}(k) = pinv(\mathbf{B}_m)\cdot\Big(\mathbf{A}_m\cdot\mathbf{x}(k) - \frac{\mathbf{x}_d(k)-\mathbf{x}_d(k-1)}{T_s} - \eta\big(\mathbf{x}_d(k)+\mathbf{x}(k)\big)\Big), \quad (58)$$

where Moore-Penrose Pseudoinverse of $\mathbf{B}_m$ is used.

ISBN: 978-1-61804-216-3

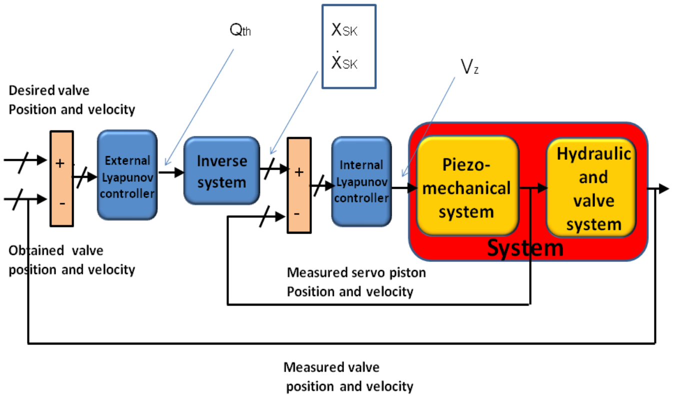

Fig. 6. Control scheme

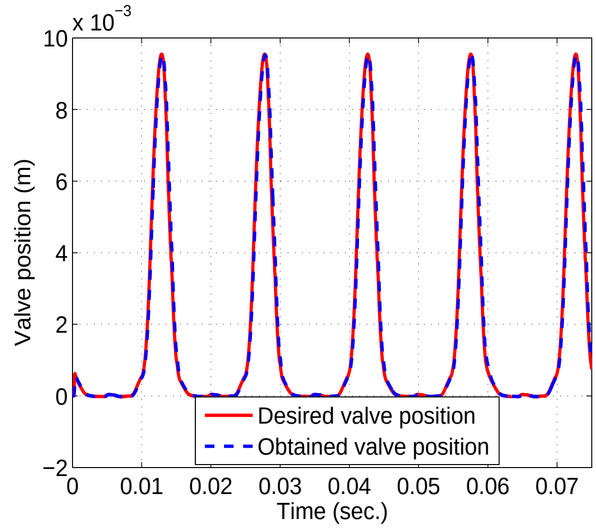

Fig. 7. Desired and obtained valve positions corresponding to 8000 rpm

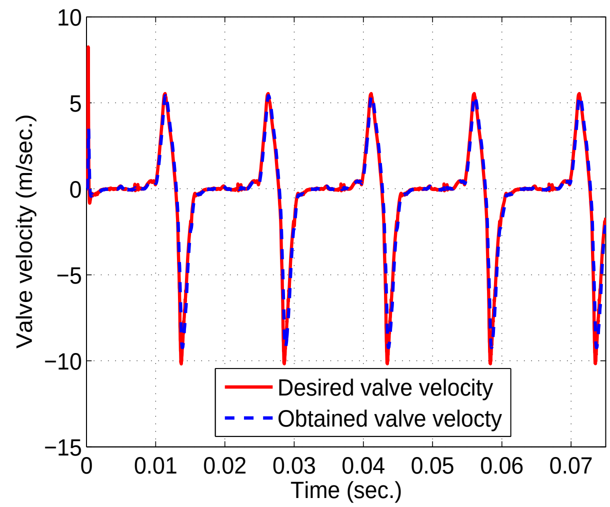

Fig. 8. Desired and obtained valve velocity considering 8000 rpm

V. Simulation results

The control scheme is shown in Fig. 6 in which the control laws of equations (38) and (58) are inside the internal and external Lyapunov blocks. After the external Lyapunov block an inversion block is put to state the algebraic relation between variable Q_{th} and variable x_{SK}. Figure 7 shows the final results concerning the tracking of a desired position of an exhaust valve with 8000 rpm. Figure 8 shows the final results concerning the tracking of a desired velocity of an exhaust valve with 8000 rpm. Concerning the force acting directly on the valve at the opening time which has a peak value equal to 700 N circa and it is reduced to a few Newton acting on the piezo part thanks to the decoupling structure of the hybrid actuator. This is one of the greatest advantages of these hybrid actuators. The model of such kind of a disturbance is obtained as an exponent function of the position of the valve. The digital controller is set to work with a sampling time equal to 20×10^{-6} s, according to the specifications of the Digital Signal Processor which we are intended to test the system with.

VI. Conclusions and future objectives

A. Conclusions

This paper deals with a hybrid actuator composed by a piezo and a hydraulic part and its control structure for camless engine motor applications. The idea is to use the advantages of both, the high precision of the piezo and the force of the hydraulic part. The proposed control scheme considers two Laypunov based controllers. Backward and Forward Euler sampling methods are compared. Simulations with real data of a motor and of a piezo actuator are shown for the controller realized by Backward Euler method.

References

[1] P. Mercorelli. An anti-saturating adaptive pre-action and a slide surface to achieve soft landing control for electromagnetic actuators. *IEEE/ASME Transactions on Mechatronics*, 17(1):76–85, 2012.

[2] P. Sarhadi, N.O. Ghahramani, and I. Shafeenejhad. Identification of a non-linear hydraulic actuator considering rate saturation using particle swarm optimisation algorithm. *In Int. J. of Modelling, Identification and Control, Inderscience publishers*, 18(2):136–145, 2013.

[3] H.J.M.T.A. Adriaens, W.L. de Koning, and R. Banning. Modeling piezo-electric actuators. *IEEE/ASME Transactions on Mechatronics*, 5(4):331–341, 2000.

[4] Y.-C. Yu and M.-K. Lee. A dynamic nonlinearity model for a piezo-actuated positioning system. In *Proceedings of the 2005 IEEE International Conference on Mechatronics, ICM* 10^{th}-12^{th} *July*, Taipei, 2005.

[5] H. Murrenhoff. *Servohydraulik*. Shaker Verlag, Aachen, 2002.